

p-Mode Oscillations in Gravitationally Highly Stratified Magnetic Solar Atmospheres

2 M. GRIFFITHS,¹ R. ERDÉLYI,^{2,3,4} R. ZHENG,⁵ AND N. GYENGE¹

3 ¹*Research IT, The University of Sheffield, 10-12 Brunswick Street, Sheffield, S10 2FN, UK.*

4 ²*Solar Physics and Space Plasma Research Centre (SP²RC), School of Mathematics and Statistics, University of Sheffield, Hicks*
Building, Hounsfield Road, S7 3RH, UK

5 ³*Department of Astronomy, Eötvös Loránd University, Pázmány P. sétány 1/A, Budapest, H-1117, Hungary*

6 ⁴*Gyula Bay Zoltán Solar Observatory (GSO), Hungarian Solar Physics Foundation (HSPF), Petőfi tér 3., Gyula, H-5700, Hungary*

7 ⁵*Shandong Key Laboratory of Optical Astronomy and Solar-Terrestrial Environment, School of Space Science and Physics, Institute of*
Space Sciences, Shandong University, Weihai, Shandong, 264209, China

10 (Received June 1, 2019; Revised January 10, 2019; Accepted September 16, 2022)

11 Submitted to AJ

12 ABSTRACT

13 The aim of the work reported in this paper is to gain understanding of the propagation characteristics
14 of p-mode oscillations in the highly gravitationally stratified magnetic solar atmosphere. An objective
15 is the measurement of the properties of the solar atmosphere and its magnetic structures. We present
16 a comparison of the analysis of results from observations and numerical simulations.

17 The paper describes 3D numerical magnetohydrodynamic (MHD) simulations of a model solar atmo-
18 sphere with a uniform vertical cylindrically symmetric magnetic field and employing simulation drivers
19 resulting in oscillations which mimic the behaviour of *p*-mode oscillations. The simulations were run
20 for different values of the magnitude of the magnetic field and a *p*-mode driver with a fixed period
21 of 300 s. For the observational study, a typical active region was selected. We report results for the
22 temporal analysis of the observational data for a region containing a small sunspot (solar pore).

23 The paper reports the variation of the energy flux and oscillation frequency of the magnetosonic
24 modes and examines their dependence on the magnetic field strength. The comparison with observa-
25 tional data indicate the presence of oscillation signals with a frequency close to that measured for the
26 simulated results.

27 We conclude that magnetic regions of the solar atmosphere are favourable regions for the propagation
28 of energy by slow magnetosonic modes. The results exhibit a frequency shift, for different values of the
29 magnetic field. The obtained periodic behaviour is confirmed by observational data, featuring similar
30 frequencies based on the intensity times series of images taken by the Solar Dynamics Observatory.

31 *Keywords:* editorials, notices — miscellaneous — catalogs — surveys

32 1. INTRODUCTION

33 Theoretical and computational studies coupled with observations from solar telescopes reveal diverse structures
34 and dynamics in the Sun's atmosphere. The culmination of these studies of the Chromosphere and the upper solar
35 atmosphere has enhanced our knowledge of the variety of magnetic field structures. Despite our armoury of observations
36 and the diverse range of computational models it still remains a challenge to make sense of this complex menagerie
37 of dynamical structures, understand solar atmospheric heating (i.e. chromospheric and coronal) and more generally
38 space weather phenomena.

39 An example of the dynamical complexity are the ubiquitous five-minute oscillations in the solar atmosphere that
40 are referred to as the solar global acoustic oscillations or *p*-modes. These global oscillations are interpreted as trapped

41 acoustic waves, i.e. standing acoustic oscillations of the solar interior. Earlier models of these oscillations assumed
 42 that there was reflection by the photosphere with at most evanescent propagation above the photosphere. It has been
 43 realised that with kinetic pressure as the restoring force, acoustic oscillations of the photosphere may be perturbed
 44 by the solar *p*-modes. There is now increasing evidence for leakage of these modes. The *p*-modes were interpreted as
 45 resonant modes trapped in a cavity formed from the steep change in density at the solar surface and a lower turning
 46 point in the interior caused by the increase in the speed of sound resulting in refraction. The physical characteristics
 47 of the solar sub-surface layers can be estimated using observations of the standing modes. The complexity and variety
 48 of magnetic structures in the solar atmosphere gives rise to a mixture of waves providing powerful diagnostics to aid
 49 our understanding and advance our knowledge.

50 Early theoretical studies reported in Roberts (1981a) and Roberts (1981b) considered wave propagation
 51 in idealised magnetic slab structures, demonstrating the fundamental conditions for MHD wave propagation.
 52 These models were soon advanced to cylindrical magnetic structures in Edwin & Roberts (1983) that addressed the
 53 conditions under which different types of MHD waves can be sustained under the conditions of the solar corona.
 54 These papers neglected gravitational stratification and focused on magnetic structuring. There was also an emphasis
 55 on the localised wave phenomena. The analysis of Campbell and Roberts (1989) investigated the role of horizontal
 56 chromospheric magnetic fields for magneto-acoustic modes. As well as finding the shift of frequencies they were also able to predict the
 57 circumstances under which different chromospheric regions would either act as a window permitting the propagation of magneto-acoustic energy, a sink where the energy is trapped or reflected back into the chromosphere.
 58 The propagation of magneto-acoustic oscillations in an isothermal atmosphere with a vertical magnetic field was investigated by Hindman et al. (1996) although small frequency shifts
 59 were accounted for, the analysis was unable to demonstrate the absorption of MHD waves, e.g. what
 60 is observed in sunspots.

61 Much of the theoretical (numerical) analysis has focused on the effect of magnetic flux tubes on
 62 wave propagation and neglected gravitational stratification. Hasan & Christensen-Dalsgaard (1992)
 63 considered an isothermal stratified atmosphere and investigated the influence of vertical fields on a
 64 variety of modes including *p*-mode oscillations. In the limit of weak fields, they were able to analyse
 65 the spectrum of oscillations in using the modes for a non-magnetised stratified atmosphere and the
 66 slow magneto-acoustic mode. The characteristics of generated waves are dependent on the motions at
 67 the footpoints of magnetic field concentrations, including those in the intergranular lanes. For example
 68 vortex motions have been demonstrated to generate Alfvén waves Fedun et al. (2009b).

69 The link between oscillations in the solar atmosphere and solar global oscillations which are the
 70 topic of the computational modelling work described in this paper is addressed by Erdélyi (2006)
 71 in a review with plenty of references. An outward propagating wave is reflected inward from the
 72 solar upper surface, or boundary layer, because of a sudden decrease in the plasma density, while the
 73 lower boundary of the cavity is formed by the increasing sound speed due to temperature rises. For
 74 global oscillation modes which exceed the acoustic cutoff frequency, there is wave leakage out from
 75 the cavity into the atmosphere. A model for understanding the behaviour of solar global oscillations
 76 based on the Klein-Gordon equation was developed by Taroyan & Erdélyi (2008). This model suggests
 77 a global resonance. Waves which are normally trapped by a frequency cut-off barrier are enhanced
 78 by a resonance enabling propagation into the upper solar atmosphere. Enhancements to the models
 79 described earlier are presented by e.g. Pintér et al. (2007), where their work utilised an exponentially
 80 decaying horizontal magnetic field as a representation of the magnetic carpet. The inhomogeneous
 81 three layer model leads to characteristic frequencies.

82 For a number of decades, intensity oscillations in the solar atmosphere have been the subject of
 83 observation and study, see Banerjee et al. (2011), De Moortel (2009), Mathioudakis et al. (2013), Ru-
 84 derman & Erdélyi (2009), Wang (2011). The observed periods of atmospheric intensity oscillations
 85 range from some seconds to several hours Auchère et al. (2014). Much earlier, it was proposed by
 86 Jensen & Orrall (1963), that the 3- and 5-minute oscillations were the characteristics of the photo-
 87 sphere and the chromosphere. Recently, the association of intensity oscillations with oscillations in
 88 coronal loops and sunspots has been confirmed for oscillation periods of three minutes. Applying solar
 89 magneto-seismology, observations of intensity observations in the solar atmosphere can be used to un-

derstand the magnetic structures in the solar atmosphere, see e.g. Roberts et al. (1984), Banerjee et al. (2007), Zaqrashvili & Murawski (2007), Erdélyi & Taroyan (2008), Verth et al. (2010). Additionally, it has been recognised that the 5-minute oscillations in loops are not related to sunspots De Moortel et al. (2002). Evidence for global oscillations is suggested by the observational analysis of Gyenge & Erdélyi (2018) that demonstrates that the frequent recurrence of micro-flare events exhibit fluctuations between 3 minutes and 12 minutes. These fluctuations arise during time intervals before and after of major solar flares.

The key point of this work is a simple comparison of numerical simulations with observations, searching for the link between ubiquitous upper atmospheric oscillations and the global solar oscillations, using our numerical representation that is of sufficient complexity to reveal the dominant dynamical processes in the magnetic solar atmosphere. Comparison of the reported observational work with the results of the modelling suggests that the sampling process is sufficient to draw such inferences.

We report the results of numerical simulations of photospheric p -mode oscillations in a model solar atmosphere with a uniform and vertical magnetic field. We also present the results of a temporal analysis based on observations of intensity oscillations with the objective of providing evidence of the existence of the temporal behaviour exhibited by our simultaneous. The work contributes to our understanding of the propagation and modification of global oscillations in the highly gravitationally stratified solar atmosphere.

First, we consider the variety of magnetic structures in the solar atmosphere and address the wave motions that are observed in these regions. This is followed with a description of the solar atmospheric model, magnetic field configuration and the simulation method we used to model p -mode oscillations in a model magnetic solar atmosphere.

2. STRUCTURES IN THE SOLAR ATMOSPHERE

There are many different kinds of structures in the highly dynamic solar chromosphere. Bright spots which form in the trenches between solar granules are known as faculae, these features which are formed near magnetic field concentrations constantly form and dissipate over time scales of several minutes. Pores are a few Mm across and they are the smaller counterparts of sunspots, they are the bright areas near to and around sunspots or faculae. The bright areas that extend away from active regions are called plage regions. The magnetic fields in this area diffuse away into the quiet Sun regions. The magnetic network is a network of lines which outline super-granules. Super-granules are convective regions about 30 Mm across, and they possess strong horizontal flows. The motions within the super-granules result in the concentration of bundles of magnetic field lines. The mean photospheric field in the inter-network region is 100-300 G. On the other hand, solar active regions contain sunspots which have sizes between 1 - 50 Mm.

Active regions producing flares may have fields which easily exceed the normal range of 100-500 G. As well as these massive concentrations, solar magnetograms reveal many north poles in the quiet photosphere, this is known as the magnetic carpet. These structures can be observed in figure 1. Along with the coronal funnels arising from grain boundaries, the picture shows a range of network loops with temperatures which can be in the range 10^5 K to 10^6 K. The dynamical phenomena of concern in this paper result in waves and oscillations in the solar atmosphere. The upward propagation of waves through the solar atmosphere can result in coronal heating, frequency shifts and other wave phenomena. A range of wave transformations may occur including reflection and refraction by atmospheric structures.

Our initial computational studies were applicable to quiet Sun regions with magnetic fluxes in the range of 5-10 G, including the non-magnetic solar chromosphere and the quiet inter-network regions between the magnetic flux concentrations. Given the variety of solar atmospheric regions, for example the network, inter network, plage and faculae regions, it is recognised that the modes of oscillation with periods of 3 and 5 minutes exhibit varying behaviour. In particular, the variation observed for different magnetic structures and reflecting layers such as the transition layer influences propagation in the upward and downward directions.

The power spectra presented in the first figure of Griffiths et al. (2018b) exhibit a variation of propagation characteristics at different levels within the solar atmosphere and within different regions such as coronal holes, the quiet sun and active regions. In general the power spectra indicate a preponderance of long period 5 minute waves with frequencies in the range 1.5-5mHz. Also observed are the distinctive peaks for the short period 3 minute waves (with

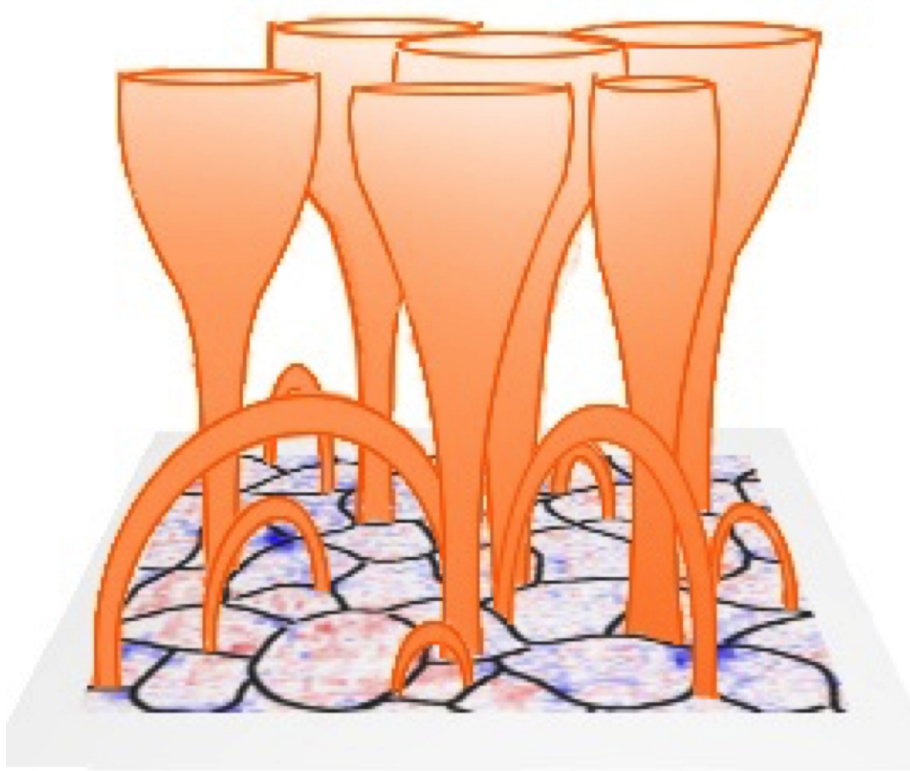


Figure 1. The schematic solar magnetic network.

144 frequencies in the range 5-8mHz). The power spectra exhibit peaks in much longer period ranges for example 12
 145 minute waves (frequencies in the range 1.1-1.5mHz) and 16 minute waves (frequencies 1-1.1mHz). For the quiet sun
 146 regions the 5 minute modes are stronger at photospheric levels and diminished higher up in the corona, but note a
 147 small peak for the data from the AIA 211 corresponding to 2.0MK.

148 The review of Khomenko and Calvo Santamaria (2013) summarises this multifaceted picture. In the close proximity
 149 of the magnetic network elements, the longer 5 minute modes propagate efficiently to the chromosphere. The 3
 150 minute modes propagate from the photosphere to the chromosphere in the network cell interiors for restricted regions
 151 of the network and internetwork. Although these long-period halos are present in the chromosphere they are most
 152 prominent in the photosphere. With their more complex magnetic structures, a more complex pattern is exhibited
 153 in plage and faculae regions. Observations show that the 3 minute modes exhibit enhancement in both photosphere
 154 and chromosphere whereas the power of the 5 minute modes increase significantly in the chromosphere. These power
 155 enhancements are known as “halos” and have been widely reported Kontogianis et al. (2010).

156 3. MOTIVATION

157 Given the complexity of the dynamics and the diversity of structures in the solar atmosphere, it is understood that
 158 a truly realistic model is challenging and requires a hybrid multi-disciplined approach. In order to develop a model
 159 providing a representation of the solar atmosphere it is necessary to establish that the modelling tools give a consistent
 160 behaviour in idealised test cases and that there is a consistency between the computational and theoretical models.
 161 Many computational MHD simulations of the sun have been undertaken, some of the approaches have resulted in an
 162 encouraging degree of realism Vögler et al. (2005), Gudiksen et al. (2011). Computational MHD simulations of the
 163 propagation of waves in 3D solar atmospheres were undertaken by Fedun et al. (2009a). Initially they considered
 164 hydrodynamical models, in later simulations Fedun et al. (2009b) Vigeesh et al. (2012) reported results for magnetized

solar atmospheres featuring an idealized flux tube. These models with point drivers demonstrated the leakage of magneto-acoustic energy into the solar atmosphere. The work of Khomenko and Calvo Santamaria (2013) and Calvo Santamaria, Khomenko and Collados (2015) reviewed and presented 2D computational MHD modelling of wave propagation in magnetic features such as sunspots and arcades.

The models reveal that vertical magnetic fields enable energy to reach the corona. Our initial models of a realistically stratified model of the solar atmosphere Griffiths et al. (2018b) were hydrodynamic simulations. In these simulations atmospheric perturbations caused by photospheric global oscillations are represented using drivers located in the photosphere so as to mimic the influence of the solar p-modes. The results of the hydrodynamic modelling exhibited agreement with the energy flux predictions from a 2 layer Klein-Gordon model. This agreement supported the interpretation of the interaction between the solar atmosphere and the global oscillations. Also revealed by the simulations was a consistency between power flux measurements from SDO and frequency dependent energy flux measurements from the numerical simulations. This observed propagation of energy into the mid to upper atmospheric regions of the quiet sun occurred for a range of frequencies. Such observations may explain observed intensity oscillations for periods greater than the well known 5-minute and 3-minute oscillations. It was also found that energy flux propagation into the lower solar corona is strongly dependent on the particular wave modes.

In this paper we present results for 3D numerical MHD simulations with an extended driver representing photospheric p-mode oscillations in a magnetic solar atmosphere, the objective is to gain understanding of the propagation characteristics of the p-mode oscillations.

4. NUMERICAL COMPUTATION METHODS

The simulations described in this paper were undertaken using the SMAUG code, a GPU implementation of the Sheffield Advanced Code (SAC) Shelyag et al. (2008). The Sheffield MHD Accelerated Using GPUs (SMAUG) Griffiths et al. (2015) and SAC are derived from the versatile advection code (VAC) developed by Tóth (1996). SAC and SMAUG are numerical MHD solvers which can be used to model the time-dependent evolution of photospheric oscillations in the solar atmosphere. The SMAUG code can simulate linear and non-linear wave propagation in strongly magnetised plasma with structuring and stratification.

We use the same general system of ideal MHD equations applicable to an ideal compressible plasma and used for our initial hydrodynamic simulations, Griffiths et al. (2018b).

$$\frac{\partial \rho}{\partial t} + \nabla \cdot (\rho \mathbf{v}) = 0, \quad (1)$$

$$\frac{\partial(\rho \mathbf{v})}{\partial t} + \nabla \cdot (\mathbf{v} \rho \mathbf{v} - \mathbf{B} \mathbf{B}) + \nabla p_t = \rho \mathbf{g}, \quad (2)$$

$$\frac{\partial e}{\partial t} + \nabla \cdot (\mathbf{v} e - \mathbf{B} \mathbf{B} \cdot \mathbf{v} + \mathbf{v} p_t) + \nabla p_t = \rho \mathbf{g} \cdot \mathbf{v}, \quad (3)$$

$$\frac{\partial \mathbf{B}}{\partial t} + \nabla \cdot (\mathbf{v} \mathbf{B} - \mathbf{B} \mathbf{v}) = 0. \quad (4)$$

The total pressure p_t is given by

$$p_t = p_k + \frac{\mathbf{B}^2}{2}, \quad (5)$$

and the kinetic pressure, p_k , is written as

$$p_k = (\gamma - 1) \left(e - \frac{\rho \mathbf{v}^2}{2} - \frac{\mathbf{B}^2}{2} \right). \quad (6)$$

In the system of equations above, \mathbf{B} is the magnetic field, \mathbf{v} is the velocity, ρ is the mass density, \mathbf{g} is the gravitational acceleration vector and e is the energy density. The SMAUG code used for the simulations reported here employs perturbed versions of the general set of MHD equations given above. For the perturbed versions the density, energy density and magnetic field are expressed in terms of perturbed and background quantities as follows

$$\rho = \tilde{\rho} + \rho_b,$$

$$e = \tilde{e} + e_b,$$

$$\mathbf{B} = \tilde{\mathbf{B}} + \mathbf{B}_b.$$

Assuming a magneto-hydrostatic equilibrium of the background plasma, the background quantities which do not change in time have a subscript b . The time varying perturbed quantities do not have a subscript. The fully non-linear MHD numerical finite element solver employs hyper-diffusion and hyper-resistivity to achieve numerical stability of the computed solution of the MHD equations Caunt and Korpi (2001). A more detailed description of the full set of MHD equations, including the hyper-diffusion source terms are given in Griffiths et al. (2015) and Shelyag et al. (2008).

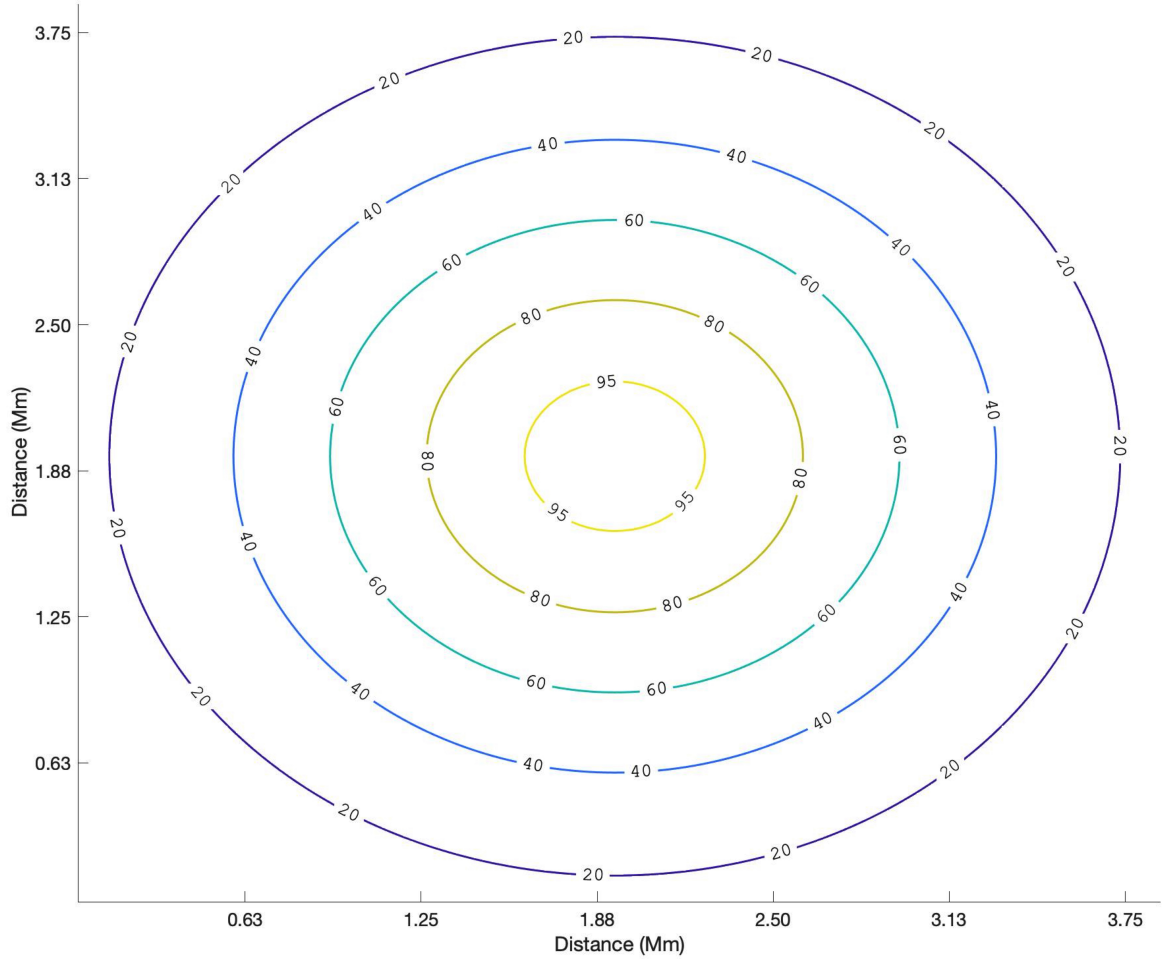


Figure 2. Initial Magnetic Field Configuration, radial field distribution, uniform in the vertical direction with a maximum value of 100G

204 5. COMPUTATIONAL MODEL

205 The hydrodynamical studies reported in Griffiths et al. (2018b) employed simulation drivers with physical characteristics
 206 representing p-mode oscillations with varying modes and periods. The MHD simulations reported here use
 207 the same driver and model of the solar atmosphere as used in our initial hydrodynamical study. The model is modified
 208 by the inclusion of a uniform, vertical and cylindrically symmetric magnetic field.

209 The dimensions of the simulation box are $L_x = 4$ Mm, $L_y = 4$ Mm and with a height of $L_z = 6$ Mm in the
 210 gravitationally stratified z -direction. The computational box is an array of elements $128 \times 128 \times 128$. The upper
 211 boundary of the model is in the solar corona whilst the lower boundary is coincident with the photosphere. The
 212 perturbed MHD code used here is suited to studying the propagation of wave energy from the photosphere, across
 213 the transition layer and leaking into the solar corona. The time scales relevant to our study are determined by the
 214 5-minute p -mode oscillations the model employs open boundary conditions thereby allowing us to model the wave
 215 propagation. To generate these oscillations we use vertical velocity drivers which are extended across the base of the
 216 model. The following sections describe the model solar atmosphere and the driver.

217 Data obtained from solar observations was used to construct a semi-empirical model solar atmosphere, the resulting
 218 model is a representation of the quiet sun. Employing the fundamental assumption of hydrostatic equilibrium, the
 219 VALIIIc model Vernazza et al. (1981) was used to construct a model of the chromosphere in equilibrium. For atmo-
 220 spheric heights greater than 2.5 Mm the results from a model of solar coronal heating were used McWhirter et al.
 221 (1975). The atmospheric profiles for temperature, density, sound speed and frequency cut-off for this model are shown
 222 in figure 5. A further possibility for a model solar atmosphere is the use of parametric models, the smoothed step
 223 function used by Murawski and Zaqrashvili (2010) is an example. Discussion of the validity of model solar atmospheres
 224 and realistic models of the chromosphere, indicate the need for observationally derived semi-empirical models,
 225 see Carlsson and Stein (1995), Kalkofen (2012). It has been suggested that local dynamo action and joule heating in
 226 the dynamical solar chromosphere make the construction of models particularly challenging Leenaarts et al. (2011).

227 For the simulations described here we use a simplistic model which is uniform in the vertical (z) direction. The
 228 cylindrically symmetric field was constructed using the parametrisation in equation 7, the effective cylinder radius was
 229 fixed at $R = 0.14$ Mm. Simulations were run for different values of B_{max} .

$$B_z = B_{max} e^{-\frac{x^2+y^2}{R^2}}, \quad (7)$$

230 Since the field is uniform in the vertical direction the model atmosphere is in magnetohydrostatic equilibrium. Details
 231 of the construction procedure for the model atmosphere, the resulting density profiles and temperature profiles are
 232 provided in Griffiths et al. (2018b).

233 6. NUMERICAL DRIVERS FOR P -MODE OSCILLATIONS

234 The work reported here is an extension of the earlier work of Malins (2007), their study represented photospheric
 235 buffeting motion using different point drivers. These studies demonstrated surface waves, structures in the transition
 236 zone and identified the effect of cut-offs induced by the stratified solar atmosphere. The overview in Section 2 identified
 237 physical phenomena delivering energy into the solar atmosphere and resulting in oscillatory behaviour.

238 The simulations presented in this paper, employ an extended driver resulting in the perturbation of the entire lower
 239 boundary of the model. Photospheric p -mode oscillations for the real sun have a horizontal wavelength and coherence.
 240 The vertical velocity driver used here is an acoustic p -mode driver located at the photosphere and exciting waves which
 241 propagate into our realistic 3D model of the solar atmosphere. An extended driver with a sinusoidal dependence and
 242 a wavelength of 8 Mm applied along the middle of the base of a computational domain of dimension 4 Mm represents
 243 a *fundamental mode*. Drivers may be constructed as an ensemble of these solar global eigenmodes. The driver is
 244 represented by the expression shown in equation (8)

$$V_z = A_{nm} \sin\left(\frac{2\pi t}{T_s}\right) \sin\left(\frac{(n+1)\pi x}{L_x}\right) \sin\left(\frac{(m+1)\pi y}{L_y}\right) \exp\left(-\frac{(z-z_0)^2}{\Delta z^2}\right), \quad (8)$$

245 For the simulations here, a p -mode driver corresponding to the 5 minute mode, was used with period 300s and mode
 246 (2,2). Earlier studies demonstrated the effectiveness of this mode with energy propagation. Simulations were run for
 247 different values of the magnitude of the magnetic field. The mode numbers identified here are the n and m values in
 248 the expression for the driver shown in equation (8).

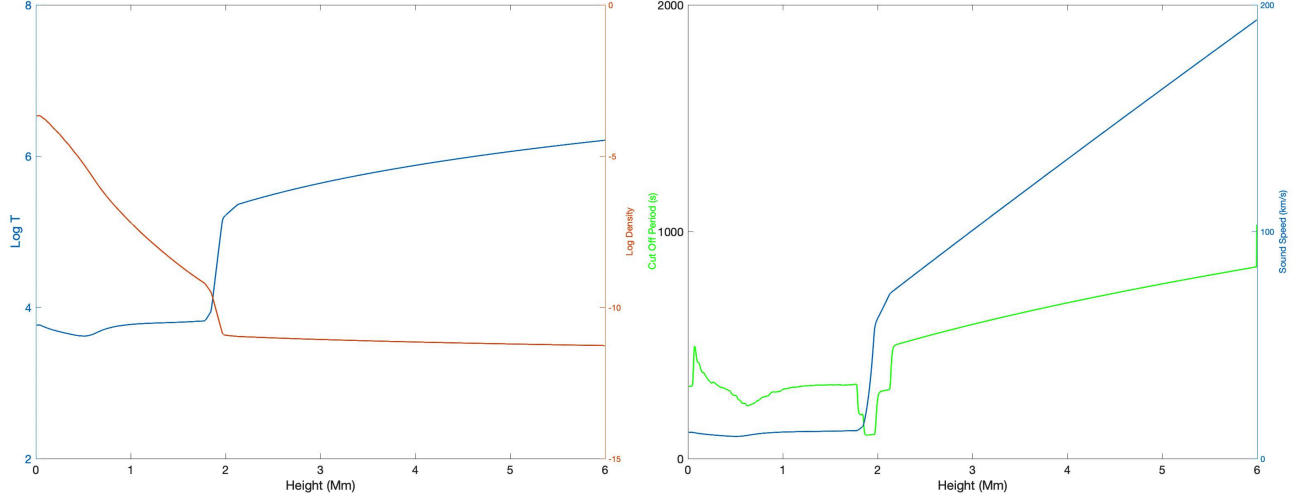


Figure 3. The left hand panel shows the temperature and density profile used for the simulations and based on the VALIIIc model. The right hand panel shows the computed soundspeed and frequency cutoff for a solar model atmosphere based on the VALIIIc model.

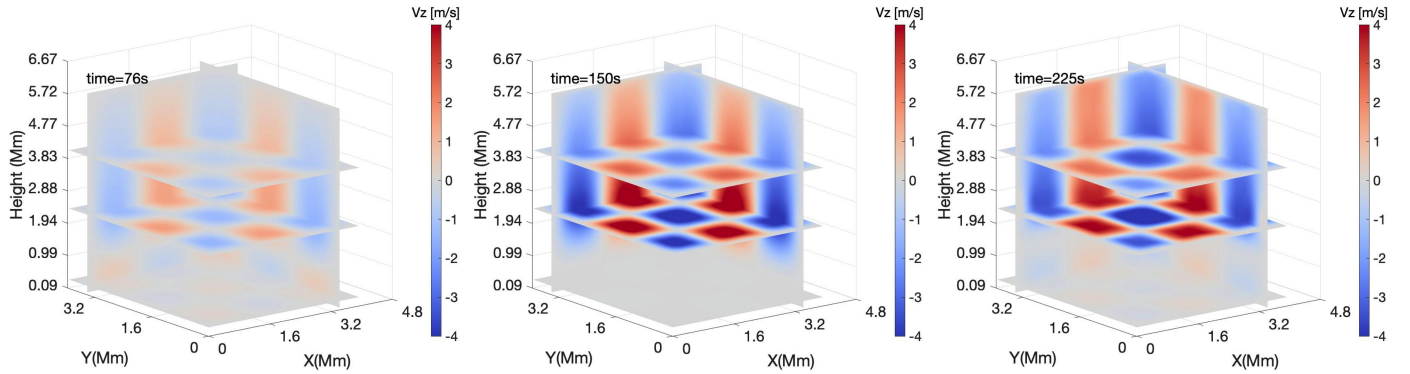


Figure 4. Vertical Component of the Velocity for Different Sections of the Simulation for 76s, 150s and 225s for a vertical field with maximum field of 100G.

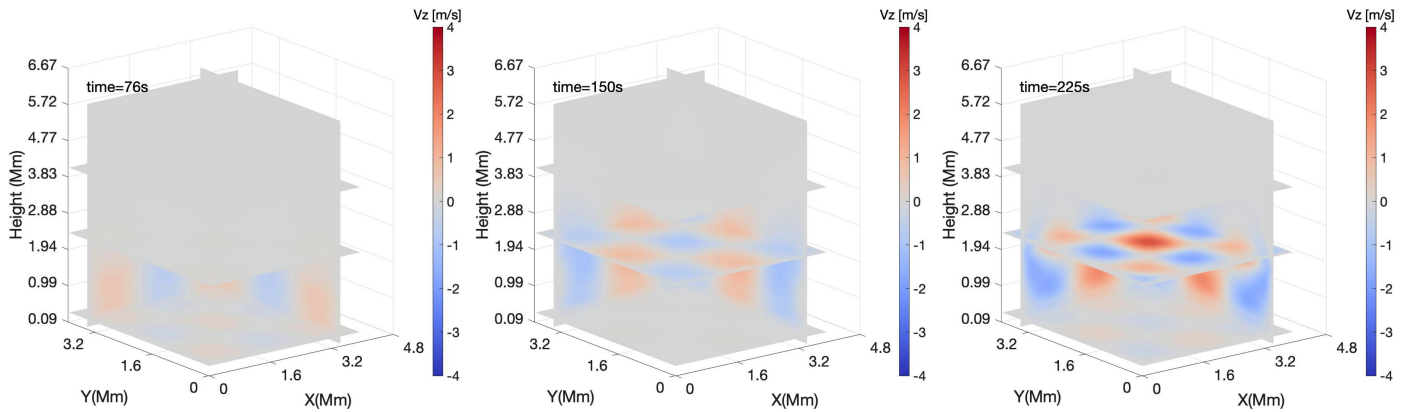


Figure 5. Vertical Component of the Velocity for Different Sections of the Simulation for 76s, 150s and 225s for a magnetic field of 0G.

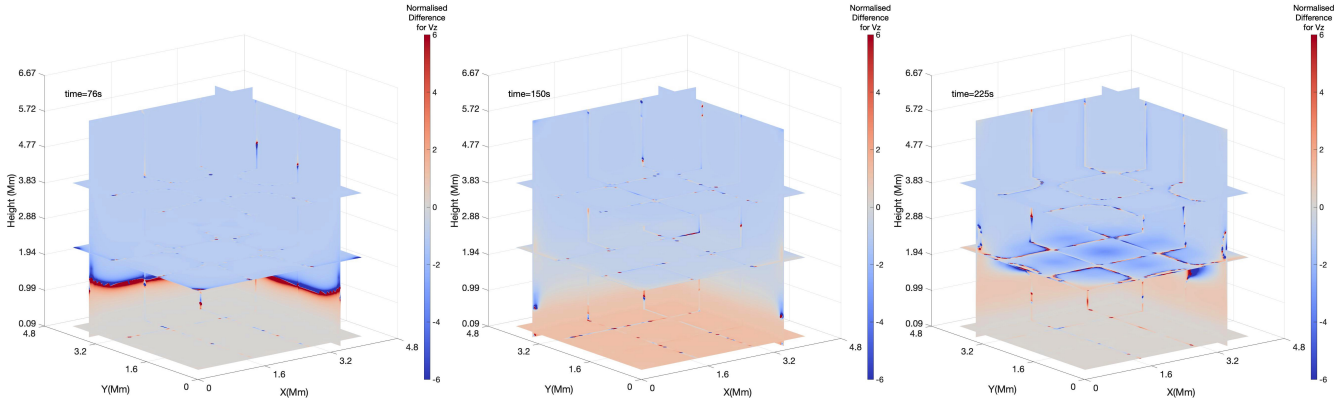


Figure 6. Normalised Difference of the Vertical Component of the Velocity for Different Sections of the Simulation for 76s, 150s and 225s for a magnetic field of 100G.

For the driver equation given in 8, T_s is the period, A_{nm} is the amplitude, the indices n and m define the mode, the lengths of the base of the simulation box in the x and y directions are L_x and L_y are respectively. The driver width, Δz is set to 4km, the parameter z_0 was set so that the vertical location of the driver is in the photosphere, coincident with the location of the temperature minimum and 0.5 Mm above the lower boundary of the model. The simulations presented use the parameter $A_{nm}=500 \text{ ms}^{-1}$ with the mode indices set to $n, m = 2$.

7. MAGNETOACOUSTIC WAVES IN UNIFORM VERTICAL MAGNETIC FIELD CONFIGURATIONS

Magnetohydrodynamic simulations have been performed with *p*-mode oscillations of the photospheric layer and for magnetic field strengths of 0G, 50G, 75G and 100G. The plasma- β for the model decreases rapidly from a value of 50 at 0.7Mm above the lower boundary of the simulation domain, β is 1 at a height of 1.39Mm. It is anticipated that for the region with $\beta \approx 1$, mode conversion occurs with full or partial conversion to magnetohydrodynamic modes. Figure 4 shows the vertical component of the velocity at various times for different sections through the simulation box. Each plot in Figure 4 corresponds to a vertical field configuration with a maximum field strength (B_{max}) of 100G. Comparison with the 0G case in Figure 5, illustrates a clear difference between the purely hydrodynamic and the MHD case. The figures for the MHD case exhibit evidence of a fast moving magneto-acoustic wave mode. The measured propagation speed is consistent with that of a fast magneto-acoustic mode. Figures 4 and 5 compare the wave modes at a quarter, half and three-quarters of a cycle.

Figure 6 shows the normalised difference between the results for the 100G case and the 0G case. The normalisation is achieved by dividing the difference value by the sum the sum of the values for the 0G and 100G case. The largest difference arises at the height where the velocity reverses direction. Our results indicated that even a small magnetic field appears to enhance the motion of plasma in the corona and there is an apparent difference in phase between the magnetic field cases. As well as an increase in the velocity amplitude with increasing magnetic field there is a small shift in the frequency of the oscillation. For magnetic fields with strengths between 1kG and 50G, the theoretical prediction of Hindman et al. (1996) resulted in frequency shifts in the microhertz and nanohertz range. Although this was a prediction of helioseismology, their result still provides insight into the mechanism of frequency shifts of waves in atmospheric magnetic structures.

A set of videos of all the simulations that were performed can be obtained from the online research data archive hosted by The University of Sheffield Griffiths et al. (2018a). The videos display the evolution of the z -component of the plasma velocity along different layers of our model solar atmosphere. Each video shows the value of the vertical component of the plasma velocity (z -component in m/s) along different slices through the simulation box. Each video is labelled using the magnetic field strength in Gauss.

A distance-time plot for the 300s period driver, with the 100G field is shown in figure 7. The wavespeeds computed from this distance-time plot are shown in table 1. The speeds for the 0G field are consistent with the speed of sound

Wave Speed (km/s)	0G	50G	75G	100G
2Mm	12.6	96.5	47.7	25.2
1Mm	10.1	64.1	44.4	45.4
0.5Mm	8.7	45.4	37.8	32.3

Table 1. The table shows wave speeds obtained from the distance-time plots for the 300s period driver with magnetic fields of 0G, 50G, 75G and 100G.

Magnetic Field (G)	1Mm	2Mm	4Mm	5.5Mm
0G	0.155	-1.771×10^{-5}	1.227×10^{-6}	8.194×10^{-7}
50G	0.270	-0.399	0.040	0.021
75G	-0.507	-0.126	0.015	0.007
100G	-0.255	-0.226	0.019	0.006

Table 2. The table shows the time averaged and integrated energy flux ratio obtained for the 300s period driver with magnetic fields of 0G, 50G, 75G and 100G.

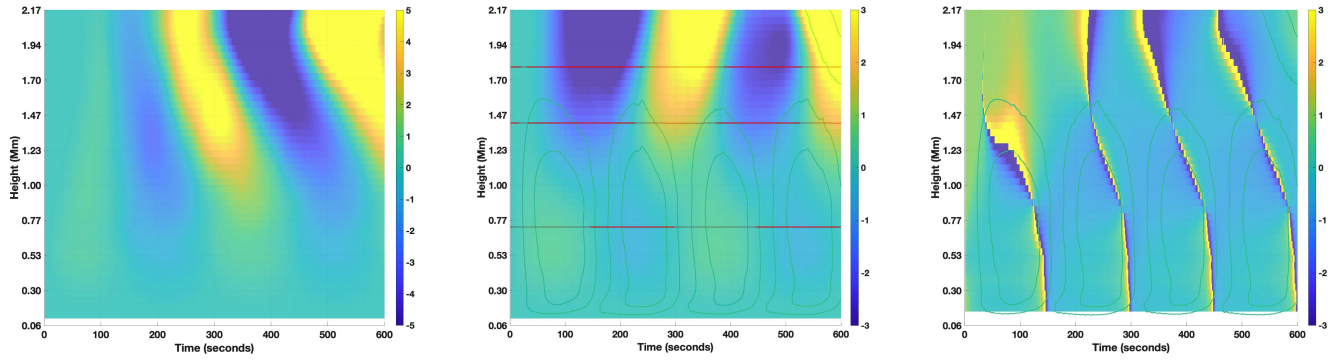


Figure 7. Distance-time plot of the vertical component of the velocity in the mid chromosphere, for the case of the difference between 0G and 100G, the central redline is the line for beta equal to 1, the lower and upper redline correspond to beta equal to 50 and 0.5 respectively.

in the solar atmosphere, whilst the speeds for the non zero magnetic field are consistent with propagation speeds for magnetosonic modes.

Investigation of figure 6 reveals excitation from the driver along with standing oscillations in the chromospheric cavity. There is also partial reflection of the signal at the boundary of the chromosphere and the transition layer. The results also display evidence for signals propagating horizontally at the transition region and with frequencies similar to that of the driver. The distance-time plot in figure 7, for the 100G case exhibits reduced reflection at the transition layer and indicates evidence for energy leakage into the solar Corona. Figure 7 shows an initial fast mode pulse followed by slow mode oscillations above the line which corresponds to a plasma β value of one. Below an height of 1Mm we observe the standing mode oscillations along with oscillations of the magnetic field perturbations. Below 0.3Mm the driver oscillations can be observed in conjunction with possible magneto-acoustic slow mode oscillations.

Since the source terms perturb only the vertical component of the velocity and the model is cylindrically symmetric, pure Alfvénic modes are not expected.

The distance-time plots and our sections displaying the vertical component of the plasma velocity indicate significant differences in the propagation behaviour for the hydrodynamic and non-zero magnetic field cases. It is necessary to understand and quantify the extent of the energy leakage into the solar atmosphere. To investigate the influence of the magnetic field on the propagation of wave energy we employ an expression for the energy flux which was used by Bogdan et al. (2003). The wave energy flux \mathbf{F}_{wave} is given by

$$\mathbf{F}_{wave} = \tilde{p}_k \mathbf{v} + \tilde{\mathbf{B}} \cdot \mathbf{B}_b \mathbf{v} + \mathbf{v} \cdot \tilde{\mathbf{B}} \mathbf{B}_b.$$

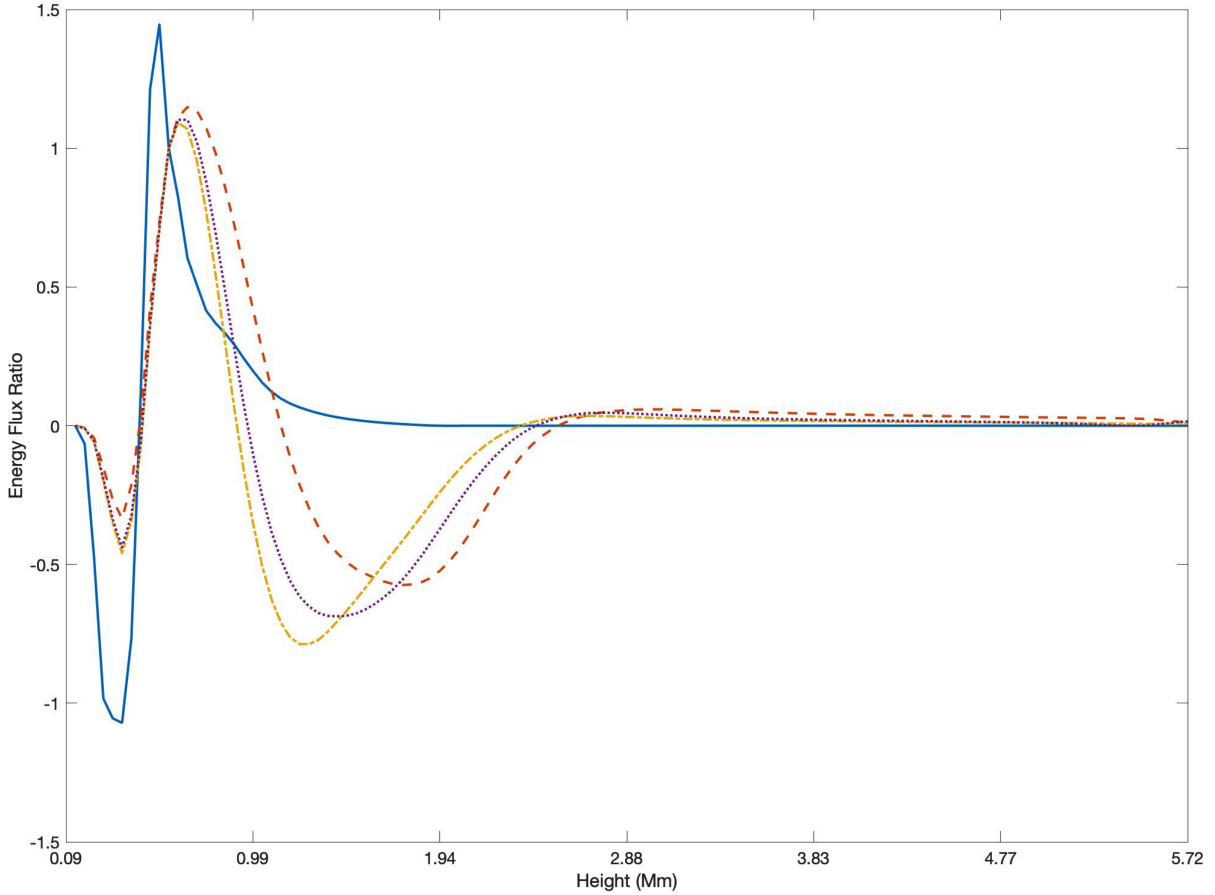


Figure 8. Shows the Ratio of the Integrated Energy Flux ratio for different values of the field, Blue 0G, Orange 50G, Purple 75 G and Red 100G.

296

We compute the time averaged energy flux integrated over different cross sections of the simulation box.

$$F_{int} = \frac{1}{t_{max}} \int_0^{t_{max}} \int \mathbf{F}_{wave} \cdot d\mathbf{A} dt, \quad (9)$$

These expressions are dependent on the perturbed kinetic pressure \tilde{p}_k .

$$\tilde{p}_k = (\gamma - 1) \left(\tilde{\epsilon} - \frac{(\tilde{\rho} + \rho_b) \mathbf{v}^2}{2} - \frac{\mathbf{B}^2}{2} \right).$$

297

298

299

300

301

302

303

304

305

306

Using equation (9), we computed the energy flux integral for each of the drivers at different atmospheric heights and averaged over the total time. We compute the ratio of this integrated energy flux to the integrated energy flux at the location of the driver. The resulting values are shown in Table 2. It appears that for heights greater than 4 Mm, the energy flux is enhanced for increasing values for the vertical magnetic field. In Figure 7, we plot the ratio of the integrated energy flux ratio for different values of the field at different heights and for the different vertical field values (the blue, orange, purple and red are for field values of 0G, 50G, 75G and 100G, respectively). These plots demonstrate that for higher B -field magnitudes there is a small leakage of energy propagation. This latter finding is interesting because this is consistent with observations and other simulation results that demonstrate an enhancement for inclined fields.

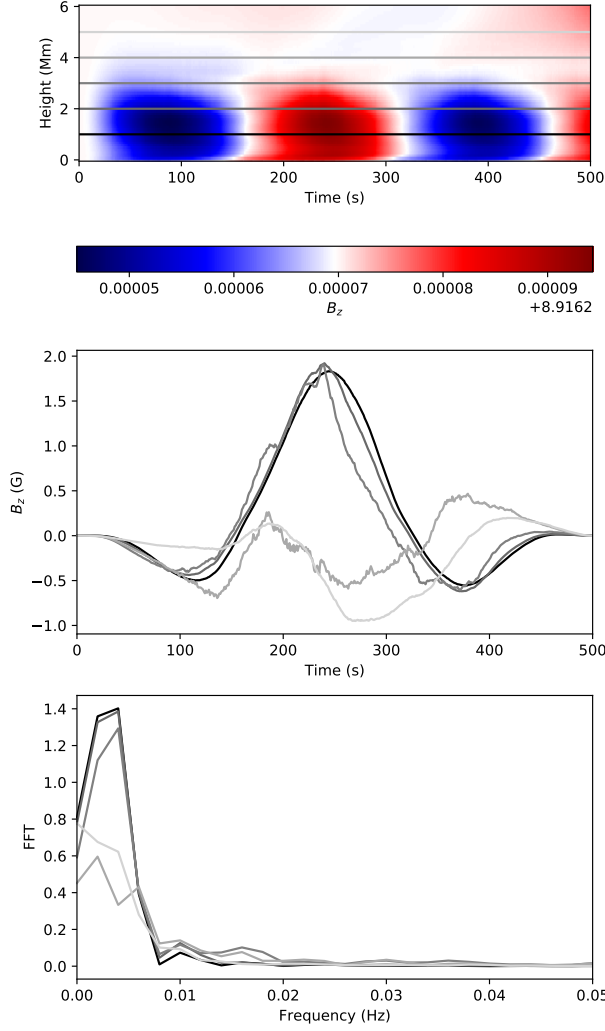


Figure 9. Temporal analysis of B_z vertical slices at 2 Mm. The top panel shows the selected vertical slices, indicated by gray colours. The middle panel demonstrates the obtained signal after applying a Hanning window function. The bottom panel shows the result of the FFT analysis based on the 5 selected vertical B_z slices.

8. FREQUENCY ANALYSIS

The top panel of Figure 9 shows a vertical slice of B_z over time. This is based on the simulation with the initial magnetic field configuration with a maximum value of 100G. The vertical axis represents the height in Mm and the horizontal axis is the time dimension, measured in seconds. From this 2-dimensional plane, 5 layers were selected, indicated by the horizontal grey lines. The middle panel of Figure 9 displays the temporal variation of the selected layers, indicated by different grey shade colours. The time series do not feature non-stationary behaviour, therefore, further transformations (such as detrending, smoothing or differentiation) are not needed. The Hanning-window function is still applied to avoid leakage effects when performing the Fast Fourier Transformation (FFT).

An FFT was applied (the lower panel) for investigating any oscillatory behaviour in the analysed signal. A significant oscillatory pattern was found with frequency range of 3.75 - 4mHz, corresponding to a period range of 4.2 - 4.4 minutes. An FFT was also performed based on the other simulations with different initial magnetic field configurations (with a maximum value of 0G , 50G, 75G and 100G). These investigations all showed similar oscillatory behaviour. Therefore, we present one FFT as a representative example. Figure 10 features the same analysis as Figure 9, however, the data is now the sample from the $B = 0$ case.

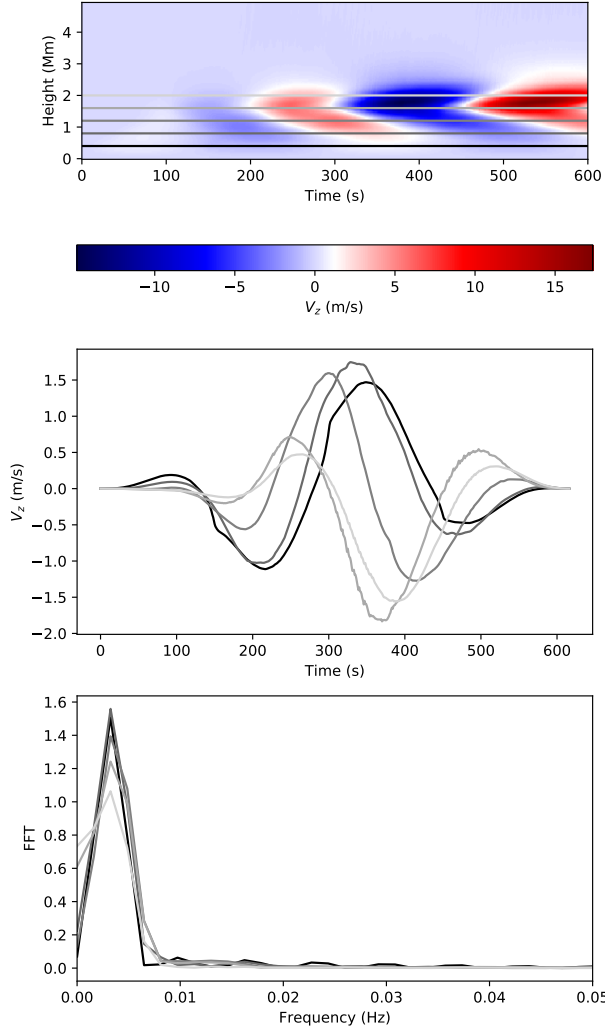


Figure 10. Temporal analysis of V_z vertical slices at 2 Mm. The top panel shows the selected vertical slices, indicated by gray colours. The middle panel demonstrates the obtained signal after applying a Hanning-window function. The bottom panel shows the result of the FFT analysis based on the 5 selected vertical V_z slices.

With the objective of confirming the obtained oscillatory behaviour, temporal analysis for the observational data was performed. We investigated intensity oscillations in the solar atmosphere observed by SDO/AIA. The passband 1600 Å was selected because our simulation mainly focused on the lower atmospheric regions, i.e. photosphere and chromosphere. The cadence of 1600 Å images is 24 seconds, therefore it was suitable for studying relatively high-frequency oscillations such as the obtained 4mHz.

The initial magnetic field configuration of our model is a standing magnetic tube, passing through the chromosphere and the lower corona. Therefore, We chose to sample a typical active region in a simplified way. The selected area contains a small sunspot (solar pore), presumably featuring similar magnetic structure as our simulation. The size of the investigated area covers 50 pixels in total, demonstrated by Figure 12. The obtained time series shows non-stationary behaviour, therefore, the observed linear trend is removed by taking the first difference Δy_t of the data. The first difference is defined as the difference between consecutive observations y_t and y_{t-1} . Furthermore, the times series is also normalised by applying standard scores (Z-scores), defined by:

$$Z_i = \frac{T_i - \bar{T}}{\sigma(T)}, \quad (10)$$

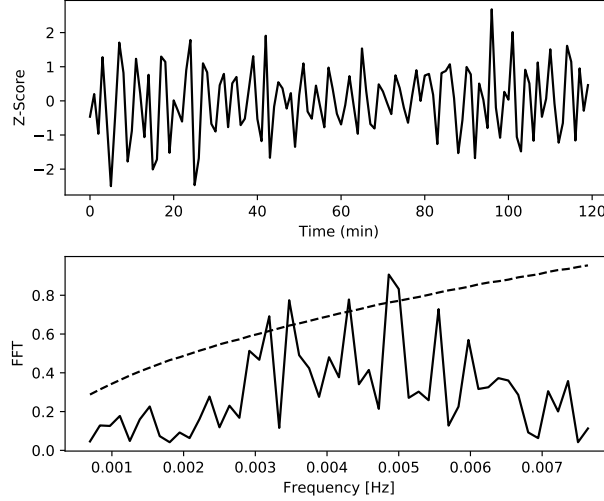


Figure 11. Temporal analysis of the intensity of a 50-pixel large area based on AIA 1600Å between 18:00 UT to 20:00 UT on 22 August 2010. The upper panel shows the temporal variation of the Z-Score (detrended and normalised pixel intensity data). The lower panel shows the FFT of the analysed observational data.

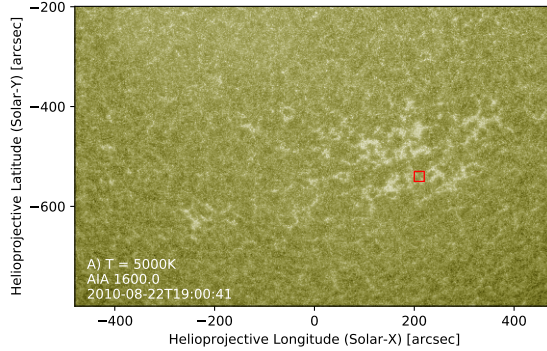


Figure 12. The selected area from the start of the investigate time series at 18:00 UT on 22 August 2010. The area is indicated by red rectangle. The size of the selected area is 50 pixels.

337 where, the parameter \bar{T} is the mean of the time series and the parameter $\sigma(T)$ is defined as the
 338 standard deviation of the data. The top panel of Figure 11 demonstrates the trend removed and
 339 normalised time series. The lower panel of Figure 11 shows the result of the applied FFT technique.
 340 The dashed line is the significance level (3σ) which was calculated using a Monte-Carlo method. The
 341 original data showed red noise signature which transformed to blue noise after differentiating the data.
 342 We have generated 1 million blue noise signatures N_b and calculated the standard deviation $\sigma(N_b)$ and
 343 the mean \bar{N}_b of the simulated noise, providing our significance level S :

$$S = \bar{N}_b + 3\sigma(N_b). \quad (11)$$

344 A significant period is found with frequency range of 3.5 – 4.2 mHz , corresponding a period range
 345 of 4 - 4.7 minutes, which is close to the period found in simulation data. Another significant peak (5
 346 mHz) is found with period around 3 minutes which may be an indication of another global oscillation.

9. CONCLUSION

348 In this paper we have presented results for a series of MHD simulations of an extended oscillator at the base of a model
 349 solar atmosphere. We have shown that energy is propagated by magnetosonic modes. Slow and fast magnetosonic
 350 modes are responsible for carrying some energy back to the chromosphere and the photosphere. The FFT analysis

demonstrated oscillatory patterns with periods in the range 4.2-4.4 minutes. This arose for both the hydrodynamic case and the case with a magnetic field of 100G, in this case there was some additional structure for the FFT analysis. These results compare favourably with the FFT analysis observations from carefully selected solar features, for example regions with pores. The results exhibit a significant shift of the frequency of these intensity oscillations from the period of the global p-mode oscillation represented in our simulations with a driver of period 5 minutes. Such shifts may be attributed to additional elasticity in the solar atmosphere resulting from the presence of a magnetic field.

Closer inspection of the energy flux propagation results are indicative of enhanced energy flux propagation for inclined magnetic fields. The obtained periodic behaviour is confirmed by observational data, featuring similar frequencies based on the intensity times series of SDO images. The results of the FFT analysis exhibit a difference with the driver frequency. The frequency difference measured from the temporal analysis of the observational and simulation data is larger than would be expected from the analysis of Hindman et al. (1996). This can be understood in part by referring to the work of Campbell and Roberts (1989).

It is encouraging that the results presented here are consistent with the behaviour exhibited by earlier work. There is an issue that due to the extended nature of the driver the amplitudes used may be responsible for delivering vast quantities of energy into the solar atmosphere and for driving a highly numerically unstable system and inducing extremely large shocks Calvo Santamaria, Khomenko and Collados (2015). Significant improvements to the comparisons presented in this paper are expected with the recent work of Kostogryz et al. (2021). Here, modelling of intensity perturbations using a VALIIIc solar atmosphere model with radiative transfer the intensity oscillations perturbed by the solar global oscillations modelled using the ADIPLS code of Christensen-Dalsgaard (2008). Also, as described in Rast & Martinez Pillet (2016), more sensitive observations with instruments such as DKIST may enable further constraints and the range of theoretical models. Future work will address simulation runs over longer time periods and for inclined fields.

10. ACKNOWLEDGMENTS

The authors thank P.H. Keys for providing the wavelet tools to analyse the related SDO data M.Korsos for the preparation of Figure 1, the Science and Technology Facilities Council (STFC) for the support they received. RE acknowledges the support received from the the Royal Society (UK). We acknowledge IT Services at The University of Sheffield for the provision of the High Performance Computing Service.

Software: SMAUG Griffiths et al. (2015), SAC Shelyag et al. (2008), VAC Tóth (1996)

REFERENCES

- Auchère, F., Bocchialini, K., Solomon, J., et al. 2014, A&A, 563, A8. doi:10.1051/0004-6361/201322572
- Banerjee, D., Erdélyi, R., Oliver, R., et al. 2007, SoPh, 246, 3. doi:10.1007/s11207-007-9029-z
- Banerjee, D., Gupta, G. R., & Teriaca, L. 2011, SSRv, 158, 267. doi:10.1007/s11214-010-9698-z
- Bogdan, T. J., Carlsson, M., Hansteen, V. H., McMurry, A., Rosenthal, C. S., Johnson, M., Petty-Powell, S., Zita, E. J., Stein, R. F., McIntosh, S. W., Nordlund, Å., 2003. Waves in the Magnetized Solar Atmosphere. II. Waves from Localized Sources in Magnetic Flux Concentrations. ApJ, 599, 626–660.
- Calvo Santamaria, I., Khomenko, E., and Collados, M., 2015. Magnetohydrodynamic wave propagation from the subphotosphere to the corona in an arcade-shaped magnetic field with a null point. A&A, 577, A70.
- Campbell, W. R. and Roberts, B. 1989. The Influence of a Chromospheric Magnetic Field on the Solar p- and f-Modes ApJ, 338, 538. doi:10.1086/167216
- Carlsson, M., Stein, R. F., 1995. Does a nonmagnetic solar chromosphere exist? ApJL, 440, L29–L32.
- Caunt, S. E., Korpi, M. J., Apr. 2001. A 3D MHD model of astrophysical flows: Algorithms, tests and parallelisation. A&A, 369, 706–728.
- Christensen-Dalsgaard, J. 2008, Ap&SS, 316, 113. doi:10.1007/s10509-007-9689-z
- De Moortel, I., Ireland, J., Hood, A. W., et al. 2002, A&A, 387, L13. doi:10.1051/0004-6361:20020436
- de Moortel, I. 2009, SSRv, 149, 65. doi:10.1007/s11214-009-9526-5
- De Moortel, I., Ireland, J., Hood, A. W., et al. 2002, A&A, 387, L13. doi:10.1051/0004-6361:20020436

- Edwin, P. M. & Roberts, B. 1983, SoPh, 88, 179.
doi:10.1007/BF00196186
- Erdélyi, R. 2006, Philosophical Transactions of the Royal Society of London Series A, 364, 351.
doi:10.1098/rsta.2005.1703
- Erdélyi, R. & Taroyan, Y. 2008, A&A, 489, L49.
doi:10.1051/0004-6361:200810263
- Fedun, V., Erdélyi, R., Shelyag, S., Sep. 2009. Oscillatory Response of the 3D Solar Atmosphere to the Leakage of Photospheric Motion. SoPh258, 219–241.
- Fedun, V., Erdélyi, R., Shelyag, S., Sep. 2009. MHD waves generated by high-frequency photospheric vortex motions. Annales Geophysicae 29, 1029–1035.
- Griffiths, M. K., Fedun, V., Erdélyi, R., 2015. A Fast MHD Code for Gravitationally Stratified Media using Graphical Processing Units: SMAUG. Journal of Astrophysics and Astronomy 36, 197–223.
- Griffiths, M., Erdélyi, R., Fedun, V., 2017. Videos of Magnetohydrodynamics Simulations of Solar Atmosphere Wave Dynamics Generated by Solar Global Oscillating Eigenmodes.
https://figshare.com/articles/Videos_of_Magnetohydrodynamics_Simulations_of_Solar_Atmosphere_Wave_Dynamics_Generated_by_Solar_Global_Oscillating_Eigenmodes/4818490
- Griffiths, M., Erdélyi, R., Fedun, V., 2018. Videos of p-Mode Oscillations in Highly Gravitationally Stratified Magnetic Solar Atmospheres.
https://figshare.shef.ac.uk/articles/dataset/Videos_of_p-Mode_Oscillations_in_Highly_Gravitationally_Stratified_Magnetic_Solar_Atmospheres/7378046
- Griffiths, M. K., Fedun, V., Erdélyi, R., and Zheng, R., 2018. Solar atmosphere wave dynamics generated by solar global oscillating eigenmodes. Advances in Space Research, 61: 720–737, January 2018.
- B. V. Gudiksen, M. Carlsson, V. H. Hansteen, W. Hayek, J. Leenaarts, and J. Martínez-Sykora. The stellar atmosphere simulation code Bifrost. Code description and validation. *A&A*, 531:A154, July 2011.
<https://doi.org/10.1051/0004-6361/201116520>.
- Gyenge, N. & Erdélyi, R. 2018, ApJ, 859, 169.
doi:10.3847/1538-4357/aac109
- Hasan, S. S. & Christensen-Dalsgaard, J. 1992, ApJ, 396, 311. doi:10.1086/171718
- Hindman, B. W. and Zweibel, E. G. and Cally, P. S., Mar. 1996. Driven Acoustic Oscillations within a Vertical Magnetic Field. ApJ459, 760–772.
- Jensen, E. & Orrall, F. Q. 1963, ApJ, 138, 252.
doi:10.1086/147631
- Kalkofen, W., 2012. The Validity of Dynamical Models of the Solar Atmosphere. SoPh276, 75–95.
- Khomenko, E., Calvo Santamaria, I., 2013. Magnetohydrodynamic waves driven by p-modes. Journal of Physics Conference Series 440 (1), 012048.
- I. Kontogiannis, G. Tsiroupolu, and K. Tziotziou. Power halo and magnetic shadow in a solar quiet region observed in the H α line. *A&A*, 510:A41, February 2010. <https://doi.org/10.1051/0004-6361/200912841>.
- Kostogryz, N. M., Fournier, D., & Gizon, L. 2021, A&A, 654, A1. doi:10.1051/0004-6361/202040264
- Leenaarts, J., Carlsson, M., Hansteen, V., Gudiksen, B. V., 2011. On the minimum temperature of the quiet solar chromosphere. A&A530, A124.
- Leighton, R. B., 1960. In: Thomas, R. N. (Ed.), Aerodynamic Phenomena in Stellar Atmospheres. Vol. 12 of IAU Symposium. pp. 321–325.
- Malins, C., 2007. On transition region convection cells in simulations of {p}-mode propagation. Astronomische Nachrichten 328, 752–755.
- Mathioudakis, M., Jess, D. B., & Erdélyi, R. 2013, SSRv, 175, 1. doi:10.1007/s11214-012-9944-7
- McWhirter, R. W. P., Thonemann, P. C., Wilson, R., 1975. The heating of the solar corona. II - A model based on energy balance. A&A40, 63–73.
- Murawski, K., Zaqrashvili, T. V., 2010. Numerical simulations of spicule formation in the solar atmosphere. A&A519, 9.
- Pintér, B., Erdélyi, R., & Goossens, M. 2007, A&A, 466, 377. doi:10.1051/0004-6361:20041632
- Rast, M. & Martinez Pillet, V. 2016, AAS/Solar Physics Division Abstracts #47
- Roberts, B. 1981a, SoPh, 69, 27. doi:10.1007/BF00151253
- Roberts, B. 1981b, SoPh, 69, 39. doi:10.1007/BF00151254
- Roberts, B., Edwin, P. M., & Benz, A. O. 1984, ApJ, 279, 857. doi:10.1086/161956
- Ruderman, M. S. & Erdélyi, R. 2009, SSRv, 149, 199. doi:10.1007/s11214-009-9535-4
- Shelyag, S., Fedun, V., Erdélyi, R., 2008. Magnetohydrodynamic code for gravitationally-stratified media. A&A486, 655–662.
- Taroyan, Y. & Erdélyi, R. 2008, SoPh, 251, 523.
doi:10.1007/s11207-008-9154-3
- Tóth, G., 1996. A General Code for Modeling MHD Flows on Parallel Computers: Versatile Advection Code. Astrophysical Letters and Communications 34, 245.
- Vernazza, J. E., Avrett, E. H., Loeser, R., 1981. Structure of the solar chromosphere. III - Models of the EUV brightness components of the quiet-sun. Astrophysical Journal Supplement Series 45, 635–725.

- 512 Verth, G., Erdélyi, R., & Goossens, M. 2010, ApJ, 714,
517 1637. doi:10.1088/0004-637X/714/2/1637
518
519
520
521
522
523
524
525
526
- 514 Vigeesh, G., Fedun, V., Hasan, S. S., Erdélyi, R., Jan. 2012.
515 Three-dimensional Simulations of Magnetohydrodynamic
516 Waves in Magnetized Solar Atmosphere. ApJ755, 1–18.
521
522
523
524
525
526
- A. Vögler, S. Shelyag, M. Schüssler, F. Cattaneo,
T. Emonet, and T. Linde. Simulations of
magneto-convection in the solar photosphere. Equations,
methods, and results of the MURaM code. *A&A*, 429:
335–351, January 2005.
<https://doi.org/10.1051/0004-6361:20041507>.
- Wang, T. 2011, SSRv, 158, 397.
doi:10.1007/s11214-010-9716-1
- Zaqarashvili, T. V. & Murawski, K. 2007, A&A, 470, 353.
doi:10.1051/0004-6361:20077246